Chemistry-driven changes strongly influence climate forcing from vegetation emissions

James Weber (j.weber@sheffield.ac.uk)
University of Sheffield https://orcid.org/0000-0003-0643-2026
Scott Archer-Nicholls
University of Cambridge
Luke Abraham
University of Cambridge
Youngsub Matthew Shin
University of Cambridge
Paul Griffiths
University of Cambridge https://orcid.org/0000-0002-1089-340X
Daniel Grosvenor
Leeds University
Catherine Scott
University of Leeds https://orcid.org/0000-0002-0187-969X
Alexander Archibald
National Centre for Atmospheric Science, University of Cambridge, Cambridge

Article

Keywords:

Posted Date: May 18th, 2022

DOI: https://doi.org/10.21203/rs.3.rs-1646168/v1

Chemistry-driven changes strongly influence climate forcing from vegetation emissions

James Weber[1*], Scott Archer-Nicholls[2], Nathan Luke Abraham[1,2], Youngsub Matthew Shin[1], Paul Griffiths[1,2], Daniel P. Grosvenor[3], Catherine E. Scott[4] and Alex T. Archibald[1,2]

[1]Centre for Atmospheric Science, Yusuf Hamied Department of Chemistry, University of Cambridge, CB2 1EW, UK
[2]National Centre for Atmospheric Science, Yusuf Hamied Department of Chemistry, University of Cambridge, Cambridge, CB2 1EW, UK
[3]National Centre for Atmospheric Sciences, School of Earth and Environment, University of Leeds, Leeds, LS2 9JT, UK
[4]School of Earth and Environment, University of Leeds, Leeds, UK

Now at: School of Biosciences, University of Sheffield, Sheffield, S10 2TN, UK

Corresponding author: James Weber
Email: j.weber@sheffield.ac.uk

Author Contributions: JW set up and executed the simulations with help from NLA, SAN, YMS and CES. JW analysed the output with input from ATA, SAN, YMS, PTG and DPG. DPG performed the offline CDNC forcing calculations.

The authors declare they have no competing interests.

Abstract

Emissions of biogenic volatile organic compounds (BVOCs) affect climate via formation of organic aerosols and their influence on cloud properties, and via atmospheric oxidation changes influencing the greenhouse gases ozone and methane. BVOCs also exhibit dependence on climate (leading to a feedback), and land use change (including afforestation/reforestation as a CO_2 removal strategy). Despite recent scientific advances, there remains considerable uncertainty between model simulations in the net impact BVOCs have on climate.

One contributor to this uncertainty is the description of BVOC chemistry, hitherto minimally assessed in a climate context. Using the Earth system model UKESM1 we quantify the influence of chemistry by comparing the climate response to a doubling of BVOC emissions in a pre-industrial atmosphere with standard and state-of-science chemistry mechanisms, with both using interactive oxidant fields. The net feedback from BVOCs is positive in UKESM1, regardless of the mechanism used. The negative feedback from enhanced aerosol scattering is outweighed by positive feedbacks from increases in ozone and methane, and changes to aerosol-cloud interactions (ACI). Contrary to prior studies, we show the ACI response is driven by reductions in cloud droplet number concentration (CDNC) via oxidant-driven suppression of gas phase SO_2 oxidation. However, with the state-of-science scheme the feedback is 43% smaller due to lower oxidant depletion yielding smaller methane increases and smaller CDNC decreases. This illustrates the significant influence of chemistry and oxidants on gas and aerosol responses to BVOC emission changes and the more complex pathways by which BVOCs influence climate than are currently recognised.

Main Text

Introduction

Atmospheric chemical composition, and its response to a perturbation, plays a key role in climate (Naik et al., 2021). Tropospheric chemistry in the current state-of-the-art climate models used in the 6th Coupled Model Intercomparison Project (CMIP6) is highly parameterised in terms of

reactions, ozone-precursor emissions, aerosol chemistry and gas-aerosol coupling and there remains considerable uncertainty in the modelling of chemistry in the lower atmosphere.

In a climatic context this uncertainty is important because tropospheric chemistry is a major factor in determining the atmosphere's oxidative capacity. Oxidants control the lifetimes of methane (CH_4), and thus its efficacy as a greenhouse gas (GHG), and a huge range of reactive gases, including volatile organic compounds (VOCs). Oxidation of VOCs in the presence of nitrogen oxides can produce ozone (O_3), another GHG. Unlike CH_4, which is well-mixed in the troposphere, O_3 is spatially heterogeneous. O_3's potency as a GHG is much greater in the cold upper troposphere (Lacis et al., 1990) and thus dependent on dispersion of O_3-precursors. Oxidants also influence aerosol processes, termed "aerosol-oxidant coupling", principally through the oxidation pathways of sulfur dioxide (SO_2) to sulfate aerosol and the oxidation of VOCs to low volatility species which can contribute to secondary organic aerosol (SOA). Aerosols influence climate directly by scattering or absorbing solar radiation and indirectly by affecting cloud properties (Boucher et al., 2013). Oxidants control where the key reactions for aerosol production occur in the atmosphere and therefore influence the resulting aerosol's lifetime, effect on cloud properties, and consequently their climatic impact (Karset et al., 2018).

Biogenic volatile organic compounds (BVOCs) play a central role in these chemistry-climate interactions. BVOCs affect climate by influencing oxidant concentrations, via direct reaction and secondary production from oxidation products (Archibald et al, 2011), and providing low volatility condensable material for SOA (e.g., Shrivastava et al., 2017). However, BVOC emissions are themselves strongly dependent on climate, leading to a BVOC-climate feedback (BCF) loop.

Feedback loops are either positive (amplifying the effect of the perturbation) or negative (opposing it). Determining both the sign and magnitude of these cycles is important to predicting future climate change (e.g., Forster et al., 2021). However, confidence in the sign and magnitude of more complex feedbacks involving multiple perturbations, which may offset, is typically low, introducing additional uncertainty in future predictions (Thornhill et al., 2021).

Emissions of BVOCs (E_{BVOC}), especially isoprene (the most widely emitted BVOC; Sindelarova et al., 2014) are strongly dependent on atmospheric conditions as well as land use change (e.g., deforestation for agriculture or reforestation for CO_2 sequestration). Rising CO_2 inhibits isoprene production (Yanez-Serrano et al., 2021) but also drives increased vegetation-mass via fertilisation (Zhu et al., 2016). The attendant higher temperatures also increase isoprene emissions exponentially up to ~38°C (Fares et al., 2011) and to a lesser extent monoterpenes (the second most widely emitted class of BVOCs). Perturbations to aerosols and cloud cover change photosynthetically active radiation (PAR) and the hydrological cycle, also influencing emissions (van Meeningen et al., 2017; Rap et al., 2018), while changes to the frequency of droughts and floods will also affect BVOC emissions (Jardine, et al., 2015). Simulated isoprene emissions exhibit increases from the present day to 2100, albeit with significant variation between both models and future climate scenarios pathways (Cao et al., 2021). Proposed re/afforestation policies would likely drive even greater increases in BVOC emissions.

The climatic impact of BVOCs has been studied with varying degrees of sophistication over the last two decades. Most studies predict that increases to SOA following enhanced E_{BVOC} would cause a negative radiative forcing (i.e a cooling) via increased aerosol scattering and cloud albedo (Carslaw et al., 2010; Scott et al., 2018a; Sporre et al., 2019), constituting a negative feedback. When changes to gas phase chemistry are also considered, the increases to CH_4 lifetime and O_3 burden cause a positive forcing (warming), although the extent to which this opposes the cooling from aerosols is uncertain. Scott et al (2018b) found the negative forcing from aerosols still outweighed the positive forcing from O_3 and CH_4 while Unger (2014), using a different model, found the opposite, concluding the presence of E_{BVOC} led to a warming. AerChemMIP also revealed significant inter-model variation in the radiative response to $2xE_{BVOC}$ (Fig.S1) with UKESM1 and GISS predicting a positive forcing dominated by increases to O_3 and CH_4 while GFDL and CESM2 a negative forcing from a larger aerosol forcing (Thornhill et al.,

2021). The impact of oxidant changes on sulfate aerosol formation resulting from increased E_{BVOC} has not previously been examined in detail and is a key factor in this work.

Thus, the uncertainty in climatic impact of BVOCs depends on the uncertainty in multiple chemical and physical processes governing the net radiative forcing. Several model studies have investigated how modelling aerosol processes (principally nucleation, condensation and growth) in different ways can affect BVOCs' climatic impact (Makkonen et al., 2012; Scott et al., 2014; Sporre at al., 2020). By contrast, there has been no rigorous assessment into the influence the description of BVOCs' gas phase chemistry, and the knock-on effects to oxidants, has on the climatic impact of BVOCs despite significant advancements in the understanding of this chemistry in the last decade (Peeters et al., 2009; Wennberg et al., 2018). For isoprene this centres on reactions of the peroxy radical formed by reaction with OH (ISOPOO). Some ISOPOO isomers can undergo intramolecular hydrogen shifts ("H-shifts") which produce species which in turn regenerate OH, termed "HO_x-recycling". These reactions increase simulated OH in isoprene-rich, NO_x-poor environments, helping to reconcile the persistent model low biases for OH against observations (Khan et al., 2020; Weber et al., 2021). We expect the smaller depletion of OH by isoprene with this chemistry to have ramifications for the atmospheric and radiative response to an E_{BVOC} perturbation via changes to CH_4, O_3, aerosol and cloud properties.

In this study we aim to assess how the description of BVOC chemistry affects the simulated climatic impact of BVOCs. We do this by examining the change to the atmosphere's composition and energy balance, specifically the radiative forcing (RF), following a doubling of E_{BVOC} in the preindustrial atmosphere (PI) using two chemical mechanisms. The RF is decomposed into components from changes to O_3, CH_4, the aerosol direct radiative effect and aerosol-cloud interactions (Methods). We highlight the multiple pathways by which chemistry, oxidants and aerosols interact to affect radiatively-active atmospheric components and thus demonstrate the importance of the uncertainty in BVOC chemistry.

Chemical Mechanisms

The scale of tropospheric chemistry (~19,000 reactions for organic species alone in the near-explicit Master Chemical Mechanism; Jenkin et al., 2015) prevents explicit simulation and necessitates the use of condensed mechanisms which reduce complexity by lumping chemical species together and considering only the most important reactions. We consider two mechanisms: Strat-Trop (ST) (Archibald et al., 2020) which is the standard mechanism in UKESM1 and designed to be practical for long climate studies, and CRI-Strat 2 (CS2) (Weber et al., 2021) which is much more comprehensive in its description of tropospheric chemistry, particularly for isoprene and monoterpenes, but more expensive to use. CS2 is based on the tropospheric chemistry scheme CRI v2.2 (Jenkin et al., 2019) which is traceable to the latest version of the MCM (v3.3.1) and conserves its ozone forming potential.

ST and CS2 are described in more detail in Methods but the major isoprene difference between the mechanisms is the inclusion of the H-shift pathways of ISOPOO (Fig.S2) in CS2. CS2 simulates 50-100% higher OH concentration in terrestrial tropical regions than ST, improving model performance for OH, isoprene and monoterpenes (Jenkin et al., 2019; Weber et al., 2021). CS2 is comparable to other more αδϖανχεδ chemical mechanisms such as the CalTech reduced isoprene scheme (Bates and Jacob., 2019) but the effect of this chemistry on the climatic impact of BVOCs has not been assessed.

For monoterpenes ST features a single tracer (MT) whose oxidation by O_3, OH and NO_3 produces only an inert species, Sec_Org_{MT}, which condenses onto aerosol or nucleates new aerosol with sulfuric acid. This lack of further chemistry means MT acts as an oxidant sink. By contrast, CS2's monoterpene chemistry features oxidation of α-pinene and β-pinene producing both Sec_Org_{MT} and other chemically active products which undergo further chemical reactions (Jenkin., 2004). The transport of these oxidation products can lead to the formation of O_3 and OH away from emission sources with associated effects on CH_4 and aerosol. The chemical treatment

of monoterpenes and the wider range of VOCs considered by CS2 means CS2's emissions of reactive organic carbon are ~180 TgC yr^{-1} (17.5%) higher than ST, leading to greater OH in the tropical planetary boundary layer (PBL; lowest ~1-2 km) and lower free troposphere (FT) (Archer-Nicholls et al., 2021).

In subsequent discussion, mechanism acronyms ST or CS2 refer to a particular detail of the mechanism (e.g. "the OH+CH_4 rate constant in ST"). Individual runs are denoted with the mechanism acronym and subscript (e.g. ST_{con}, ST_{2x} for the control run and run with doubled BVOC ($2xE_{BVOC}$) respectively). ST_Δ and $CS2_\Delta$ refer to the change between the control and $2xE_{BVOC}$ simulations for a given parameter (e.g., "the change in O_3 in ST_Δ" refers to the change in O_3 for ST_{2x} - ST_{con}) (Methods).

Results

Fig. 1 shows the RF, radiative efficiency and feedback factor from changes in O_3 ($SARF_{O3}$), CH_4, aerosol scattering (IRF_{DRE}) and the interactions of clouds with radiation, termed the cloud radiative effect (CRE) (Methods). Both mechanisms simulate a net positive radiative forcing (and therefore a positive feedback), but the forcing in $CS2_\Delta$ (168±33 mWm^{-2}) is 43% smaller than ST_Δ (298±37 mWm^{-2}). This is driven by smaller positive forcings from CH_4 (-45 mWm^{-2}; -16%) and CRE (-92 mWm^{-2}; -50%) in $CS2_\Delta$ compared to ST_Δ which, along with the 8% smaller $SARF_{O3}$ (-8 mWm^{-2}), outweigh the 7% (16 mWm^{-2}) stronger negative IRF_{DRE} in ST_Δ. The negative IRF_{DRE} and positive CH_4 and $SARF_{O3}$ forcings following an E_{BVOC} increase are qualitatively in agreement with prior studies (e.g., Unger 2014; Thornhill et al., 2021), but the positive CRE contrasts with most studies: Scott et al (2018b) and Sporre et al (2019) both simulated negative CRE with increased E_{BVOC}. The key processes controlling these forcings and the factors driving the mechanistic differences are now reviewed.

Discussion

The Hydroxyl Radical & Methane

The larger positive CH_4 forcing in ST_Δ than $CS2_\Delta$ can be understood with reference to changes in the OH concentration. $2xE_{BVOC}$ depletes OH throughout the troposphere in both ST_{2X} and $CS2_{2X}$ but the relative reduction is larger in ST_Δ of -31% (cf. -24% in $CS2_\Delta$) is one of the fundamental causes of the different climatic responses between the chemical mechanisms. In the lowest 5 km, OH decreases by >65% (>55%) and >50% (>35%) over Amazonia and central Africa respectively in ST_Δ ($CS2_\Delta$), two of the regions with greatest BVOC emissions (Fig.2(a,b)). In the lowest ~1 km CS2's enhanced HO_x-recycling from isoprene is particularly influential while in the lower tropical FT (~1-5 km) the mechanistic differences come from a greater increase OH production from HO_2+NO and hydroperoxide (ROOH) photolysis in $CS2_\Delta$.

CS2 produces higher yields of the major hydroperoxide (H_2O_2) than ST from the ozonolysis of isoprene (38.5% vs. 9%). The consideration of monoterpene chemistry in CS2, in contrast to ST, also leads to higher production of H_2O_2 (18% direct yield vs. zero in ST) and as well as HO_2-precursors (e.g., HCHO). Thus, $2xE_{BVOC}$ produces a greater increase in H_2O_2 and HO_2 in $CS2_\Delta$ than ST_Δ, driving a greater increase in secondary OH production in the lower FT (Fig.S3(a,b)).

As the major tropospheric sink for CH_4, the decrease in OH following $2xE_{BVOC}$ leads to reductions in CH_4 oxidation and increases in simulated CH_4 concentration. The reduction in oxidation flux is greatest in the warm tropical lower troposphere (Fig.2(c)) given the large OH reduction and strong positive temperature dependence of OH+CH_4. The larger reduction of OH in ST_Δ leads to a larger decrease in CH_4 oxidation flux (Fig.2(d)), corresponding to larger increases in CH_4 concentration

(ST_Δ 276 ppbv vs. $CS2_\Delta$ 223 ppbv) and forcing (ST_Δ 275 mWm^{-2} vs. $CS2_\Delta$ 230 mWm^{-2}) (Methods).

Ozone

The forcing from O_3 changes is dictated by the partitioning of nitrogen between reactive NO_x and reservoir species (predominantly peroxyacetylnitrate (PAN) and nitric acid ($HONO_2$)), the availability of peroxy radical (RO_2) precursors and the location of O_3 production: the radiative efficiency of O_3 (forcing per unit change in concentration) is greater around the tropical tropopause than in the lower troposphere (Lacis et al., 1990).

$2xE_{BVOC}$ reduces PBL O_3 over the major biogenic emission regions via O_3's direct reaction with BVOCs. PAN formation also increases but mechanistic differences mean PAN has a ~35% longer lifetime in the warm PBL in ST than CS2. This leads to greater vertical transport of PAN into the FT where the lower temperature increases PAN's lifetime (from ~1 hr in the PBL to ~2 days in the FT).

The increase in PAN in the middle troposphere in both mechanisms leads to lower NO_x throughout the region and a reduction in O_3, greater in ST_Δ. However, around the tropical tropopause, increases in HO_2, driven by the photolysis of carbonyls such as HCHO produced from BVOC oxidation products, result in increased O_3 via the reaction of HO_2 + NO and subsequent NO_2 photolysis. The increase in HO_2, and thus O_3, is greater in ST_Δ since the greater reduction of OH leads to greater vertical transport of these HO_2 precursors, allowing them to reach the region with maximum O_3 radiative efficiency. By contrast, HO_2 production from carbonyl photolysis increases by more in $CS2_\Delta$ in the lower and middle tropical troposphere where O_3's radiative efficiency is lower (Fig.2(e,f)).

The result is an 8% smaller forcing in $CS2_\Delta$ (92±9 mWm^{-2}) compared to ST_Δ (100±10 mWm^{-2}) despite $CS2_\Delta$ producing a 20% greater increase in tropospheric O_3 burden; highlighting the influence of O_3 precursor-transport and thus oxidant concentrations.

Aerosol Scattering (IRF_{DRE})

The increase in E_{BVOC} not only increases the fuel for SOA production (and thus burden), but also, via oxidant depletion, influences the location of SOA production. The reduction in OH (Fig.2(a,b)) increases BVOC lifetimes meaning SOA-precursors are formed at higher altitude, further from E_{BVOC} sources, and the resulting SOA has a longer lifetime and greater climatic impact. The greater OH reduction in ST_Δ yields greater increases in isoprene lifetime (8.2 hr (66%) vs. 3.7 hr (61%)) and thus transport away from source than in $CS2_\Delta$. Accordingly, SOA burden (lifetime) increases by 121% (12%) in ST_Δ compared to 114% (7%) in $CS2_\Delta$. The greater vertical transport of SOA-precursors in ST_Δ also means SOA concentrations increases by more in the FT in ST_Δ and in the PBL for $CS2_\Delta$ (Fig. 3(a)) while column SOA increases are greater over E_{BVOC} source regions in $CS2_\Delta$ and over more remote regions, particularly the central Atlantic, in ST_Δ (Fig.3(b)).

ST_Δ and $CS2_\Delta$ also differ in how the extra SOA-precursors alter the SOA size and number distribution. The greater increase of precursors within the PBL in $CS2_\Delta$ results in a larger increase in condensation to accumulation mode particles than in ST_Δ. Conversely, the greater transport of precursors into the FT in ST_Δ means condensation flux to the Aitken mode increases by a greater extent. In turn this yields a greater increase in accumulation number concentration in ST_Δ, via growth of Aitken particles to accumulation mode size, over much of Amazonia, central Africa and the central Atlantic.

The differences in SOA dispersion and accumulation mode number concentration between ST_Δ and $CS2_\Delta$ have direct consequences for the spatial changes in aerosol scattering and the attendant forcing. The statistically significant (95% confidence) IRF_{DRE} is slightly stronger over Amazonia and central Africa in $CS2_\Delta$ but noticeably stronger over the central Atlantic in ST_Δ

(Fig.3(c,d)), correlating well with the difference in SOA column and aerosol number concentration. The IRF_{DRE} is the single largest forcing component and the greater dispersion of additional SOA in ST_{Δ} leads to a 7% stronger forcing (-260 vs. -244 mWm^{-2}). Similarly, Sporre et al (2020) found that following a doubling of SOA, greater transport of SOA in the EC-Earth model compared to NorESM and ECCHAM led to a stronger IRF_{DRE}.

Cloud Forcing (CRE)

In ST_{Δ} and $CS2_{\Delta}$ SOA increases drive higher cloud droplet number concentration (CDNC) over Amazonia and over the central Atlantic (Fig.3(e,f)) (downwind of central Africa) following the spatial change of SOA accumulation mode aerosol, although much of the CDNC increase is not statistically significant (95% confidence).

However, statistically significant decreases in CDNC occur over large areas of the south Atlantic, south Pacific and Southern Ocean (Fig.3(e,f)), regions downwind of the Amazon (Putnam and Sokolowsky., 2014) and with high stratocumulus coverage (Wood., 2012). This is driven by sulfate aerosol changes, not SOA, and the response in ST_{Δ} is much stronger than in $CS2_{\Delta}$ (Fig.3(e,f)). Co-located increases in cloud droplet effective radius are also simulated and, for a given cloud liquid water content, such changes reduce cloud albedo (Twomey., 1974). Accordingly, both mechanisms simulate positive global SW CRE (ST_{Δ} 222 mWm^{-2}, $CS2_{\Delta}$ 137 mWm^{-2}). Offline calculations isolating the impact of CDNC changes (Grosvenor and Carslaw., 2020, Methods) also find reductions in outgoing SW radiative flux (i.e., positive forcings) over the south Atlantic and Southern Ocean (Fig.3(g,h)).

The CDNC decreases are driven by reduction in gas phase oxidation of SO_2 by OH to form H_2SO_4 which in turn nucleates new aerosol particles. The suppression of H_2SO_4 production is greater in ST_{Δ} (3.0 vs. 2.0 Tg yr^{-1}) due to the greater reduction in OH. The reduction in H_2SO_4 production and thus new particle nucleation (25 Gg yr^{-1} ST_{Δ} vs. 14 Gg yr^{-1} $CS2_{\Delta}$) (Fig.S4) leads to compensatory increases in aqueous phase SO_2 oxidation by H_2O_2, which only adds mass to existing particles predominantly in the accumulation mode (whereas nucleation adds to aerosol mass and number). The increase in aqueous SO_2 oxidation is reinforced by the increases in H_2O_2 from the additional BVOC loading.

The net effect is a shift in the aerosol size distribution to fewer, larger particles. Accordingly, ST_{Δ} exhibits a 26% decrease in Aitken mode SO_4 burden compared to 21% in $CS2_{\Delta}$, particularly downwind of the major biogenic emission regions (e.g., south Atlantic from Amazonia), and a more widespread decrease in Aitken mode number concentrations. Larger Aitken mode particles can activate to cloud condensation nuclei (CCN) in remote regions (Sporre et al., 2020) and so their decrease reduces CDNC concentrations. The LW component of the CRE is small and very similar between the mechanisms but the net CRE of 183 mWm^{-2} in ST_{Δ} compared to 91 mWm^{-2} in $CS2_{\Delta}$ constitutes the largest difference between the mechanisms among the forcing components.

The central role of oxidants

Fig. 4 contrasts the feedback loops which arise when model simulations consider the impact of BVOC emissions (a) solely from aerosol changes and (b) when chemistry and oxidants change as well. The latter yields a more complex response and highlights the central role of oxidants in influencing not only the forcing from gas phase composition changes but from aerosol and cloud property changes too.

The most noticeable difference between these paradigms is the sign of the CRE which is negative in (a) but positive in (b). This illustrates the subtle difference between the IRF_{DRE} and CRE from a perturbation to E_{BVOC} with interactive oxidants (as done here) and the IRF_{DRE} and CRE from a perturbation to SOA or E_{BVOC} with prescribed oxidants (e.g., Scott et al., 2014; Sporre

et al., 2019 respectively). In the latter case, the only way an E_{BVOC} or SOA increase can impact ACI is via changes to SOA which typically results in a negative CRE typically (although not always, cf. EC-Earth in Sporre et al., 2020) by providing additional condensable mass which grows aerosol particles to sizes where they can act as cloud condensation nuclei and therefore increase CDNC, with a minor contribution from enhanced aerosol nucleation. This tends to make BVOCs appear strong cooling agents. When simulating a doubling of CO_2, Sporre et al (2019) found the total negative aerosol forcing (direct and CRE) from the accompanying E_{BVOC} increase offset 13% of the positive forcing from CO_2. This substantial offsetting arose from a very strong positive dependence of E_{BVOC} on temperature (highest among AerChemMIP models) causing a large increase in SOA which yielded strong negative forcings, particularly from CRE, with no concomitant oxidant-driven forcing from changes to sulfate aerosol, O_3 and CH_4.

By contrast, the use of interactive oxidants here not only results in radiatively-important changes to O_3 and CH_4 but also changes in SOA transport (affecting IRF_{DRE}) and significant perturbations to sulfate aerosol via reduction in gas phase SO_2 oxidation. This reduces new particle formation and CDNC, yielding a positive CRE which outweighs the impact of increased SOA and leads to the opposite conclusion to Sporre et al (2019).

The link between oxidants, CDNC and CRE has also been simulated in O'Connor et al (2021) where OH-suppression from increases to CH_4 concentration yielded CDNC reductions and a positive CRE. However, the impact of increased H_2O_2 (substantial from BVOC increases but less so from CH_4 increases) favouring aqueous phase SO_2 oxidation further highlights the even wider range of pathways via which BVOCs can affect climate.

Fully understanding the climatic impact of BVOC emissions requires capturing as many of these oxidant-influenced interactions as possible. This is particularly important in the context of nature-based climate policies since incorrectly diagnosing their effects on climate could lead to implementation of ineffective or even counterproductive policies.

Conclusions

Changes to CO_2 concentration, climate (temperature, flooding, droughts) and land use policies, including well-intentioned efforts to promote biodiversity and mitigate climate change by increasing CO_2 sequestration (via re/afforestation or energy crops), will affect future BVOC emissions in a complex manner. Understanding how these changes will influence climate change is therefore critical for reducing uncertainty in future climate projections and ensuring that such mitigation policies are beneficial and not counterproductive.

Increasing emissions of BVOCs leads to a cascade of chemical and climatic impacts in the Earth system. Increases in BVOCs drive complex changes in the distribution of oxidants with concomitant effects on the burden and lifetime of radiatively important gases, aerosols and cloud properties. In a PI climate, a doubling of E_{BVOC} in UKESM1 leads to increases in O_3 and CH_4 and decreases to CDNC/cloud albedo through a reduction in gas phase SO_2 oxidation. In ST, the combined positive forcing from these changes outweighs the negative forcing arising from the scattering of radiation from enhanced SOA, yielding a positive feedback.

However, when a state-of-the-science chemistry scheme (CS2), featuring recent developments in isoprene chemistry, is used the net positive BCF is 43% smaller. The central driver of this difference is a smaller reduction in oxidants and attendant smaller increases in CH_4 and smaller decreases in gas phase SO_2 oxidation, CDNC and cloud albedo. The smaller oxidant depletion also limits the transport of O_3-precursors up to the upper-troposphere, where O_3 is most potent as a GHG, yielding a smaller positive forcing despite a greater increase in tropospheric O_3 burden. The wide-scale transport of SOA from the enhanced E_{BVOC} is lower in CS2 following the lower oxidant depletion, yielding a smaller negative aerosol and cloud forcing, but this effect is outweighed by the diminished positive forcings from CH_4, cloud albedo and O_3.

While most prior work on the climatic impact of BVOCs has focused on the impact to aerosols and the accompanying uncertainty in BVOC-aerosol parameterisations, this work demonstrates the important coupling between aerosols, chemistry and oxidants. The necessity of using interactive (rather than prescribed) oxidants in the context of the BVOC feedback has already been demonstrated by the radiatively-important changes to O_3 and CH_4 (e.g. Thornhill et al., 2021). By comparing the response to an E_{BVOC} increase with two interactive chemical mechanisms, this study progresses beyond prior studies by identifying the wider reach of oxidants as they impact not only the forcing from gas phase composition changes but also the forcing from aerosol and cloud property changes; previously overlooked interactions. The strong dependence of the BVOC feedback on oxidants, and therefore the chemical mechanism, demonstrates the importance of accurately representing tropospheric chemistry for determining the influence of BVOCs on climate. Change to atmospheric chemical composition is not the only way re/afforestation as a CO_2 removal policy will influence climate: perturbations to land surface albedo, oceanic CO_2 exchange and the hydrological cycle, including cloud formation, are also important factors (Boysen et al., 2020). Nevertheless, understanding how BVOC emission changes will affect climate is essential for assessing the viability of this strategy.

Materials and Methods

Model Runs

All model runs were performed for 45 years (15 years spin up, 30 years analysis) with pre-industrial timeslice conditions using the UKESM1-AMIP setup at a horizontal resolution of 1.25° x 1.875° with 85 vertical levels up to 85 km (Walters et al., 2019). All simulations had fully interactive stratospheric and tropospheric chemistry, including interactive oxidants, using either the Strat-Trop (ST) mechanism (Archibald et al., 2020) or the CRI-STRAT 2 (CS2) mechanism (Weber et al., 2021). The simulations used the GLOMAP-mode aerosol scheme which simulates sulfate (SO_4), sea-salt (SS), black carbon (BC), primary organic aerosol (POA), secondary organic aerosol (SOA) and dust but not nitrate aerosol (Mann et al., 2010, Mulcahy et al., 2020). In this setup, the model tracks the mass concentration of each mode present in each component (e.g. SO_4 nucleation mode) and the total particle number concentration for the nucleation, Aitken (soluble and insoluble), accumulation and coarse modes.

Emissions of well-mixed greenhouse gases (WMGHGs), such as methane (CH_4) and CO_2, were not simulated; rather, prescribed lower boundary conditions at PI levels were applied for CO_2 (284 ppm), CH_4 (808 ppb) and N_2O (273 ppb), consistent with control runs of UKESM1's contributions to AerChemMIP (Collins et al., 2017).

The setup of these runs followed the AerChemMIP protocol (Collins et al., 2017) to allow calculation of the ERF. Fields for SSTs, SI, ocean biogeochemistry (DMS and chlorophyll) and land cover were taken from monthly mean climatologies derived from 30 years of output of the UKESM1 fully-coupled pre-industrial control experiment (piControl) discussed in Sellar et al (2019). Timeslice PI anthropogenic and biomass burning emissions were taken from the CEDS dataset (Hoesly et al., 2018) and van Marle et al (2017) respectively. While the atmosphere-only setup with fixed SSTs does constrain the wider Earth system response (for example aerosol-driven changes to PAR cannot change land cover via fertilisation of additional vegetation), it does reduce the noise which would occur with a coupled ocean. Importantly it also allows this study's results to be directly comparable to other studies such as the emission perturbation runs in AerChemMIP. The use of ERF, as opposed to other definitions of radiative forcing such as instantaneous radiative forcing, allows the inclusion of stratospheric temperature adjustments but also rapid adjustments in the troposphere including temperature, water vapour, clouds, and land surface temperature (O'Connor et al., 2021).

All terrestrial biogenic emissions, except isoprene and MT, were based on 2001-2010 climatologies from Model of Emissions of Gases and Aerosols from Nature under the Monitoring

Atmospheric Composition and Climate project (MEGAN-MACC) version 2.1 (Guenther et al., 2012). Oceanic emissions were from the POET 1990 dataset (Olivier et al., 2003). Oceanic DMS emissions were calculated from seawater DMS concentrations (Sellar et al., 2019) which were prescribed from the fully coupled UKESM1 PI control run.

As in the UKESM1 runs for AerChemMIP, isoprene and MT emissions were calculated using the iBVOC emissions system (Pacifico et al., 2011) which calculates the emissions interactively based on temperature, CO_2, plant functional type and photosynthetic activity. The use of iBVOC allows for a more faithful estimate of pre-industrial emissions of biogenic species compared to using present-day emissions inventories such as MEGAN-MACC (Sindelarova et al., 2014) since iBVOC considers the PI land use and atmospheric conditions such as lower CO_2. In the CS2 runs, the MT emissions calculated by the iBVOC system were split into α-pinene and β-pinene in a 2:1 ratio as in previous studies using the CRI mechanisms (Archer-Nicholls et al., 2021, Weber et al., 2021).

Chemical Mechanisms

The Strat-Trop and CRI-Strat 2 chemical mechanisms are described in detail in Archibald et al (2020) and Weber et al (2021) respectively. ST features isoprene chemistry from Pöschl et al (2000) where ISOPOO forms the isoprene hydroperoxide (ISOPOOH) via reaction with HO_2 and methacrolein the major product from reaction of ISOPOO with NO, NO_3 and other peroxy radicals (RO_2). By contrast, CS2 also features the H-shift reactions of ISOPOO and more comprehensive treatment of organonitrates.

The rate constant for the reaction of MT+NO_3 in ST was corrected from the erroneously high expression of $1.19\times10^{-12}e^{925/T}$ to $1.19\times10^{-12}e^{490/T}$, bringing it into line with the IUPAC preferred value (https://iupac-aeris.ipsl.fr/htdocs/datasheets/pdf/NO3_VOC9_NO3_apinene.pdf, last accessed 14th September 2021) for α-pinene on which the ST tracer MT is based. This results in a reduction in the rate constant of ~80%, but as NO_3 is a minor sink for monoterpenes, this change does not have a huge impact on aerosol formation.

SOA scheme improvements

The UKESM1 contributions to AerChemMIP (which also used the Strat-Trop chemical mechanism) simulated SOA production only from monoterpene oxidation with a doubled molar yield of 26% (28.6% mass yield) to account for the lack of SOA production principally from isoprene but also other VOCs (Mulcahy et al., 2020). However, as a greater fraction of monoterpenes are produced in high latitude forests compared to isoprene (Sindelarova et al., 2014), this approach skewed SOA production to higher latitudes with implications for SOA lifetime and climatic impact. Nucleation of new particles from the clustering of oxidised organic species and sulfuric acid was also omitted in the UKESM1 simulations for AerChemMIP.

In this current study, the description of SOA was improved from that used by UKESM1 in AerChemMIP to include SOA production from isoprene as well as monoterpenes and aerosol nucleation in the boundary layer from Sec_Org_{MT} and H_2SO_4 (Methods). Inert SOA-precursors were produced from monoterpenes (Sec_Org_{MT}) at the original molar yield of 13% (14.3% mass yield) (Equation 1) and isoprene (Sec_Org_{Isop} 3% molar yield; 3.3% mass yield) (Equation 2). SOA-precursors from both species could condense onto existing aerosol while nucleation of new particles via the clustering of H_2SO_4 and Sec_Org_{MT} was also simulated following the scheme of Metzger et al(2010) (Equation 3) but constrained to the model boundary layer. The inclusion of isoprene SOA and boundary layer nucleation (BLN) represent improvements over the standard UKESM1 model setup used for AerChemMIP (e.g., Thornhill et al., 2021).

$$MT + O_x \rightarrow 0.13\ Sec\_Org_{MT} \rightarrow \text{Condensation or Nucleation} \quad (1)$$

$$\text{Isoprene} + O_x \rightarrow 0.03\ Sec\_Org_{ISOP} \rightarrow \text{Condensation} \quad (2)$$

$$J = k[H_2SO_4][Sec\_Org_{MT}] \text{ where } k = 5 \times 10^{-13} \text{ molecules cm}^{-3}\ s^{-1} \quad (3)$$

(O_x = OH, O_3 or NO_3)

The change in SOA precursor yields leads to total organic aerosol (primary + secondary) burdens which are 9% and 17% higher in the ST_{con} and ST_{2x} simulations in this study compared to the corresponding PI control and $2xE_{BVOC}$ UKESM1 simulations in AerChemMIP.

Forcing Definitions
For each mechanism pair, the ERF is defined as the difference in TOA net radiative flux (Equation 4)

$$\mathrm{ERF} = \Delta\mathrm{N} = \mathrm{N}_{2x} - \mathrm{N}_{\mathrm{con}} \quad (4)$$

Following the approach of Ghan (2013) and O'Connor et al (2021), the ERF can be decomposed in aerosol direct radiative effects (IRF_{DRE}) (Equation 5), aerosol-cloud effects (CRE) (Equation 6), and clear-sky effects (CS) (Equation 7).

$$\mathrm{IRF}_{\mathrm{DRE}} = \Delta(\mathrm{N} - \mathrm{N}_{\mathrm{clean}}) \quad (5)$$
$$\Delta\mathrm{CRE} = \Delta\left(\mathrm{N}_{\mathrm{clean}} - \mathrm{N}_{\mathrm{clear,\ clean}}\right) \quad (6)$$
$$\mathrm{ERF}_{\mathrm{CS}} = \Delta\left(\mathrm{N}_{\mathrm{clear,\ clean}}\right) \quad (7)$$

$\mathrm{N}_{\mathrm{clean}}$ is the net flux excluding scattering and absorption by aerosols, and, $\mathrm{N}_{\mathrm{clear,clean}}$ is the flux excluding scattering and absorption by aerosols and clouds. Thus, the IRF_{DRE} corresponds to the difference in net TOA radiative flux due solely to the scattering and absorption of aerosols (changes to land surface albedo are negligible due to prescribed land use) while the CRE reflects changes to cloud forcing via aerosol indirect effects. The clear sky forcing corresponds to change due to the absorption and emission of radiation by gas phase species.

The prescribed surface concentration of CH_4 in the model setup significantly constrains the response of CH_4 concentrations to oxidant perturbations and thus the radiative effect. However, the change in CH_4 concentration which would have occurred had surface CH_4 concentration not been constrained can be diagnosed (Equation 8).

$$\frac{\Delta\mathrm{C}}{\mathrm{C}} = \left(\frac{\Delta\tau}{\tau} + 1\right)^{\mathrm{f}} - 1 \quad (8)$$

Where C is the CH_4 concentration, τ is the methane lifetime and f is the feedback of methane on its own lifetime (Fiore et al., 2009) taken as 1.28 for the pre-industrial period (O'Connor et al., 2020). The forcing due to the change in CH_4 concentration was then calculated using the approach in Etminan et al (2016) using the baseline concentrations of CH_4 and N_2O of 808 ppb and 273 ppb respectively. Following Thornhill et al (2021), this forcing was then scaled by 1.52 to account for the additional chemical production of ozone and stratospheric water vapour.

Unlike methane, O_3 concentrations can respond to changes in E_{BVOC}, and the resulting forcing is included in the clear sky forcing component, $\mathrm{ERF}_{\mathrm{CS}}$. The forcing from ozone changes was isolated using the radiative kernel from Skeie et al (2020) as in Thornhill et al (2021).

Offline CDNC Forcing Calculation
Offline radiative flux calculations were performed to calculate the forcing due to changes in CDNC alone (ERF_{CDNC}). Monthly mean values were used for all variables for these calculations. This followed the technique described in Grosvenor et al (2017) and Grosvenor and Carslaw (2020) for TOA fluxes and used CDNC, total cloud fraction (f_c, calculated using maximum random overlap), in-cloud (as opposed to all-sky) liquid water path (LWP_{ic}), SW clear-sky upwelling flux at TOA ($\mathrm{F}_{\mathrm{SW}}^{\mathrm{clear-sky}}$), SW downwelling flux at TOA ($\mathrm{F}_{\mathrm{sw,down}}$) and the surface albedo (A_{surf}) as inputs.

The approach used here differs slightly to those studies due to the inclusion here of $F_{SW}^{clear-sky}$ from the model for the clear-sky regions rather than assuming a constant transmissivity. A transmissivity of 0.89 was use above cloud. Multiple scattering between the surface and cloud was also included here following Seinfeld and Pandis (2006). A_{surf} was calculated by dividing the upwelling clear-sky SW surface fluxes by the corresponding downwelling fluxes. $LWP_{in\text{-}cloud}$ is the LWP from the cloudy regions only and was calculated by dividing the all-sky LWP data (as output by the model) by f_c (e.g., as in Seethala and Horváth., 2010).

ERF_{CDNC} was calculated firstly by using the control ("con") values as a baseline for the SW TOA flux (F_{SW}) calculation and then calculating the difference between this and an F_{sw} value calculated using the 2x BVOC ("2x") values for CDNC and control values for everything else (Equation 9).

$$\begin{aligned} ERF_{CDNC,con\ base} = {} & F_{SW}\left(CDNC_{2x}, f_{c,con}, LWP_{ic,con}, F_{SW,con}^{clear-sky}, F_{SW,down,con}, A_{surf,con}\right) \\ & - F_{SW}\left(CDNC_{con}, f_{c,con}, LWP_{ic,con}, F_{SW,con}^{clear-sky}, F_{SW,down,con}, A_{surf,con}\right) \end{aligned} \quad (9)$$

Then the 2xBVOC run was used as a baseline and the CDNC from the control substituted in Equation 10.

$$\begin{aligned} ERF_{CDNC,2x\ base} = {} & F_{SW}\left(CDNC_{2x}, f_{c,2x}, LWP_{ic,2x}, F_{SW,2x}^{clear-sky}, F_{SW,down,2x}, A_{surf,2x}\right) \\ & - F_{SW}\left(CDNC_{con}, f_{c,2x}, LWP_{ic,2x}, F_{SW,2x}^{clear-sky}, F_{SW,down,2x}, A_{surf,2x}\right) \end{aligned} \quad (10)$$

An overall value for ERF_{CDNC} was calculated as the average of $ERF_{CDNC,con\ base}$ and $ERF_{CDNC,\ 2x\ base}$.

Feedback Factor

For a given forcing ΔF, the resultant change to TOA radiative imbalance, ΔN, can be expressed by $\Delta N = \Delta F + \alpha \Delta T$ where α is the climate feedback parameter and represents the rate of change of the TOA radiative imbalance with respect to the global mean change in surface temperature, ΔT. α can be decomposed into individual feedback terms, α_i, arising from changes to different climate variables, C_i (Equation 11).

$$\alpha = \frac{d\Delta N}{d\Delta T} = \sum_i \frac{\partial \Delta N}{\partial \Delta C_i} \frac{\partial \Delta C_i}{\partial \Delta T} = \sum_i \alpha_i \quad (11)$$

In this study the climate variable of interest is E_{BVOC}. The corresponding feedback factor, α_{BVOC}, can be considered as the forcing arising from the change in E_{BVOC} in response to a temperature change (Equation 12).

$$\alpha_{BVOC} = \frac{\partial \Delta N}{\partial \Delta E_{BVOC}} \frac{\partial \Delta E_{BVOC}}{\partial \Delta T} = \phi_{BVOC} \gamma_{BVOC} \quad (12)$$

Where ϕ_{BVOC} is the radiative efficiency per unit change in emissions (i.e., the change in TOA radiative imbalance per unit change in emissions with typical units of Wm^{-2} $(Tg\ yr^{-1})^{-1}$) and γ_{BVOC} is the change in E_{BVOC} with climate ($Tg\ yr^{-1}\ K^{-1}$).

ϕ_{BVOC} is calculated by dividing the radiative forcing diagnosed from the timeslice model simulation pairs (ST_{con} & ST_{2x}, $CS2_{con}$ & $CS2_{2x}$) by the change in emissions.

γ_{BVOC} is diagnosed from a pair of timeslice model simulations: the piControl which simulates an 1850s atmosphere and the abrupt-4xCO_2 which is initialised from the piControl before atmospheric CO_2 concentrations are instantly quadrupled. These simulations were run for 150 years as part of the AerChemMIP project (Collins et al., 2017) and the changes in temperature and emissions were calculated from the mean of years 121-150. The change in E_{BVOC} per unit temperature change was then calculated.

Nomenclature

The terms used to represent the response of an atmospheric parameter for a given mechanism are defined in Equations 13 and 14 while Equation 15 shows the difference between two responses.

$$ST_{\Delta} = ST_{2x} - ST_{con} \quad (13)$$

$$CS2_{\Delta} = CS2_{2x} - CS2_{con} \quad (14)$$

$$CS2_{\Delta} - ST_{\Delta} = (CS2_{2x} - CS2_{con}) - (ST_{2x} - ST_{con}) \quad (15)$$

Acknowledgements

James Weber was funded by a Vice-Chancellor's Award from the Cambridge Trust. Scott Archer-Nicholls and Alex T. Archibald have been funded by NERC PROMOTE (grant no. NE/P016383/1). Nathan Luke Abraham and Alex T. Archibald are supported by NERC and NCAS through the ACSIS project. Youngsub M. Shin has been funded by NERC through the University of Cambridge ESS-DTP.

This work used Monsoon2, a collaborative high-performance computing facility funded by the Met Office and the Natural Environment Research Council. This work used JASMIN, the UK collaborative data analysis facility.

Author Contributions

JW set up and executed the simulations with help from NLA, SAN, YMS and CES. JW analysed the output with input from ATA, SAN, YMS, PTG and DPG. DPG performed the offline CDNC forcing calculations.

Data Availability

The data from the UKESM1 simulations is available from the University of Cambridge ATTO's repository at https://doi.org/10.17863/CAM.83526.

References

1. V. Naik et al. Climate Change 2021: The Physical Science Basis. Contribution of Working Group I to the Sixth Assessment Report of the Intergovernmental Panel on Climate Change. Masson-Delmotte, V., P. Zhai, A. Pirani, S. L. Connors, C. Péan, S. Berger, N. Caud, Y. Chen, L. Goldfarb, M. I. Gomis, M. Huang, K. Leitzell, E. Lonnoy, J. B. R. Matthews, T. K. Maycock, T. Waterfield, O. Yelekçi, R. Yu and B. Zhou (eds.)]. (Cambridge University Press, 2021).

2. A.A. Lacis, D.J. Wuebbles and J.A. Logan. Radiative forcing of climate by changes in the vertical distribution of ozone. *Journal of Geophysical Research: Atmospheres*, 95, 9971-9981 (1990).

3. O. Boucher et al. Clouds and Aerosols. In: Climate Change 2013: The Physical Science Basis. Contribution of Working Group I to the Fifth Assessment Report of the Intergovernmental Panel on

Climate Change. [Stocker, T.F., D. Qin, G.-K. Plattner, M. Tignor, S.K. Allen, J. Boschung, A. Nauels, Y. Xia, V. Bex and P.M. Midgley (eds.)]. (Cambridge University Press, 2013) pp. 571–658.

4. I.H. Karset et al. Strong impacts on aerosol indirect effects from historical oxidant changes, *Atmos. Chem. Phys.,* 18, 7669–7690 (2018).

5. A.T. Archibald et al. Impacts of HOx regeneration and recycling in the oxidation of isoprene: Consequences for the composition of past, present and future atmospheres. *Geophysical Research Letters*, 38, (2011).

6. M. Shrivastava et al. Recent advances in understanding secondary organic aerosol: Implications for global climate forcing." *Reviews of Geophysics* 55.2, 509-559 (2017).

7. P. Forster et al. Climate Change 2021: The Physical Science Basis. Contribution of Working Group I to the Sixth Assessment Report of the Intergovernmental Panel on Climate Change. [Masson-Delmotte, V., P. Zhai, A. Pirani, S. L. Connors, C. Péan, S. Berger, N. Caud, Y. Chen, L. Goldfarb, M. I. Gomis, M. Huang, K. Leitzell, E. Lonnoy, J. B. R. Matthews, T. K. Maycock, T. Waterfield, O. Yelekçi, R. Yu and B. Zhou (eds.)]. (Cambridge University Press, 2013).

8. G. Thornhill et al. Climate-driven chemistry and aerosol feedbacks in CMIP6 Earth system models. *Atmospheric Chemistry and Physics* 21.2, 1105-1126 (2021).

9. K. Sindelarova, et al. Global data set of biogenic VOC emissions calculated by the MEGAN model over the last 30 years. *Atmospheric Chemistry and Physics* 14.17 9317-9341 (2014).

10. A.M. Yáñez-Serrano et al. Dynamics of volatile organic compounds in a western Mediterranean oak forest. *Atmospheric Environment* 257, 118447 (2021).

11. Z. Zhu et al. Greening of the Earth and its drivers. *Nature climate change* 6.8, 791-795 (2016).

12. Y. van Meeningenet al. Isoprenoid emission variation of Norway spruce across a European latitudinal transect. *Atmospheric Environment* 170 45-57 (2017).

13. A. Rap et al. Enhanced global primary production by biogenic aerosol via diffuse radiation fertilization. *Nature Geoscience* 11.9, 640-644 (2018).

14. K.J. Jardine et al. Green leaf volatile emissions during high temperature and drought stress in a central amazon rainforest. *Plants* 4.3, 678-690 (2015).

15. Y. Cao et al. Ensemble projection of global isoprene emissions by the end of 21st century using CMIP6 models. *Atmospheric Environment* 267, 118766 (2021).

16. K.S. Carslaw et al. A review of natural aerosol interactions and feedbacks within the Earth system. *Atmospheric Chemistry and Physics* 10.4, 1701-1737 (2010).

17. C.E. Scott et al. Substantial large-scale feedbacks between natural aerosols and climate. *Nature Geoscience* 11.1, 44-48 (2018a).

18. M.K. Sporre et al. BVOC–aerosol–climate feedbacks investigated using NorESM. *Atmospheric Chemistry and Physics* 19.7, 4763-4782 (2019).

19. C.E. Scott et al. Impact on short-lived climate forcers increases projected warming due to deforestation. *Nature communications* 9.1, 1-9 (2018).

20. N. Unger. On the role of plant volatiles in anthropogenic global climate change. *Geophysical Research Letters* 41.23, 8563-8569 (2014).

21. R. Makkonen et al. BVOC-aerosol-climate interactions in the global aerosol-climate model ECHAM5. 5-HAM2. *Atmospheric Chemistry and Physics* 12.21, 10077-10096 (2012).

22. C.E. Scott et al. The direct and indirect radiative effects of biogenic secondary organic aerosol. *Atmospheric Chemistry and Physics* 14.1, 447-470 (2014).

23. M.K. Sporre et al. Large difference in aerosol radiative effects from BVOC-SOA treatment in three Earth system models. *Atmospheric Chemistry and Physics* 20.14, 8953-8973 (2020).

24. J. Peeters et al. HOx radical regeneration in the oxidation of isoprene. *Physical Chemistry Chemical Physics* 11.28, 5935-5939 (2009).

25. P.O. Wennberg et al. Gas-phase reactions of isoprene and its major oxidation products. *Chemical reviews* 118.7, 3337-3390 (2018).

26. M.A.H. Khan et al. Changes to simulated global atmospheric composition resulting from recent revisions to isoprene oxidation chemistry. *Atmospheric Environment* 244, 117914 (2021).

27. J. Weber et al. Improvements to the representation of BVOC chemistry–climate interactions in UKCA (v11. 5) with the CRI-Strat 2 mechanism: incorporation and evaluation. *Geoscientific Model Development* 14.8, 5239-5268 (2021).

28. M. E. Jenkin, J.C. Young and A.R. Rickard. The MCM v3. 3.1 degradation scheme for isoprene. *Atmospheric Chemistry and Physics* 15.20, 11433-11459 (2015).

29. A.T. Archibald et al. Description and evaluation of the UKCA stratosphere–troposphere chemistry scheme (StratTrop vn 1.0) implemented in UKESM1. *Geoscientific Model Development* 13.3, 1223-1266 (2020).

30. M.E. Jenkin et al. The CRI v2. 2 reduced degradation scheme for isoprene. *Atmospheric Environment* 212, 172-182 (2019).

31. K.H Bates and D.J Jacob. A new model mechanism for atmospheric oxidation of isoprene: global effects on oxidants, nitrogen oxides, organic products, and secondary organic aerosol. *Atmospheric Chemistry and Physics*, *19*(14), 9613-9640 (2019).

32. M.E. Jenkin. Modelling the formation and composition of secondary organic aerosol from α- and β-pinene ozonolysis using MCM v3. *Atmospheric Chemistry and Physics* 4.7,1741-1757 (2004).

33. S. Archer-Nicholls et al. The Common Representative Intermediates Mechanism version 2 in the United Kingdom Chemistry and Aerosols Model. *Journal of Advances in Modeling Earth Systems* 13.5, e2020MS002420 (2021).

34. W. Putnam and E. Sokolowsky. NASA's Goddard Space Flight Center/Global Modeling and Assimilation Office. https://svs.gsfc.nasa.gov/30637, accessed 18th March 2022 (2014).

35. R. Wood. Stratocumulus clouds. *Monthly Weather Review* 140.8, 2373-2423 (2012).

36. D.P. Grosvenor and K.S. Carslaw. The decomposition of cloud–aerosol forcing in the UK Earth System Model (UKESM1). *Atmospheric Chemistry and Physics* 20.24, 15681-15724 (2020).

37. F.M. O'Connor et al. Assessment of pre-industrial to present-day anthropogenic climate forcing in UKESM1. *Atmospheric Chemistry and Physics* 21.2, 1211-1243 (2021).

38. L.R. Boysen et al. Global climate response to idealized deforestation in CMIP6 models. *Biogeosciences* 17.22, 5615-5638 (2020).

39. D. Walters et al. The Met Office Unified Model global atmosphere 7.0/7.1 and JULES global land 7.0 configurations. *Geoscientific Model Development* 12.5, 1909-1963 (2019).

40. G.W. Mann et al. Description and evaluation of GLOMAP-mode: A modal global aerosol microphysics model for the UKCA composition-climate model. *Geoscientific Model Development* 3.2, 519-551 (2010).

41. J.P. Mulcahy et al. Description and evaluation of aerosol in UKESM1 and HadGEM3-GC3. 1 CMIP6 historical simulations. *Geoscientific Model Development* 13.12, 6383-6423 (2020).

42. W.J. Collins et al. AerChemMIP: quantifying the effects of chemistry and aerosols in CMIP6. *Geoscientific Model Development* 10.2, 585-607 (2017).

43. A.A. Sellar et al. UKESM1: Description and evaluation of the UK Earth System Model. *Journal of Advances in Modeling Earth Systems* 11.12, 4513-4558 (2019).

44. R.M. Hoesly et al. Historical (1750–2014) anthropogenic emissions of reactive gases and aerosols from the Community Emissions Data System (CEDS). *Geoscientific Model Development* 11.1, 369-408 (2018).

45. M. Van Marle et al. Historic global biomass burning emissions for CMIP6 (BB4CMIP) based on merging satellite observations with proxies and fire models (1750–2015). *Geoscientific Model Development* 10.9, 3329-3357 (2017).

46. A.B. Guenther et al. The Model of Emissions of Gases and Aerosols from Nature version 2.1 (MEGAN2. 1): an extended and updated framework for modeling biogenic emissions. *Geoscientific Model Development* 5.6, 1471-1492 (2012).

47. J.G.J. Olivier et al: Present and future surface emissions of atmospheric compounds, POET Report #3, EU project EVK2-1999-00011, available at: http://www.aero.jussieu.fr/projet/ACCENT/Documents/del2_final.doc (2003)

48. F. Pacifico et al. Evaluation of a photosynthesis-based biogenic isoprene emission scheme in JULES and simulation of isoprene emissions under present-day climate conditions. *Atmospheric Chemistry and Physics* 11.9, 4371-4389 (2011).

49. U. Pöschl et al. Development and intercomparison of condensed isoprene oxidation mechanisms for global atmospheric modeling. *Journal of Atmospheric Chemistry*37.1 29-52 (2000).

50. S. Metzger et al. Gas/aerosol partitioning: 1. A computationally efficient model. *Journal of Geophysical Research: Atmospheres* 107.D16, ACH-16 (2002).

51. S.J. Ghan. Estimating aerosol effects on cloud radiative forcing. *Atmospheric Chemistry and Physics* 13.19, 9971-9974, 2013.

52. A.M. Fiore et al. Multimodel estimates of intercontinental source-receptor relationships for ozone pollution. *Journal of Geophysical Research: Atmospheres*114.D4 (2009).

53. M. Etminan et al. Radiative forcing of carbon dioxide, methane, and nitrous oxide: A significant revision of the methane radiative forcing. *Geophysical Research Letters* 43.24 12-614 (2016).

54. R.B. Skeie et al. Historical total ozone radiative forcing derived from CMIP6 simulations. *Npj Climate and Atmospheric Science* 3.1,1-10 (2020).

55. D.P. Grosvenor et al. The relative importance of macrophysical and cloud albedo changes for aerosol-induced radiative effects in closed-cell stratocumulus: insight from the modelling of a case study. *Atmospheric Chemistry and Physics* 17.8, 5155-5183 (2017).

56. J.H. Seinfeld and S.N. Pandis. Atmospheric Chemistry and Physics: From Air Pollution to Climate Change. 2nd Edition, (John Wiley & Sons, New York, 2006).

57. C. Seethala and A. Horváth. Global assessment of AMSR-E and MODIS cloud liquid water path retrievals in warm oceanic clouds. *Journal of Geophysical Research: Atmospheres* 115.D13 (2010).

Figures and Tables

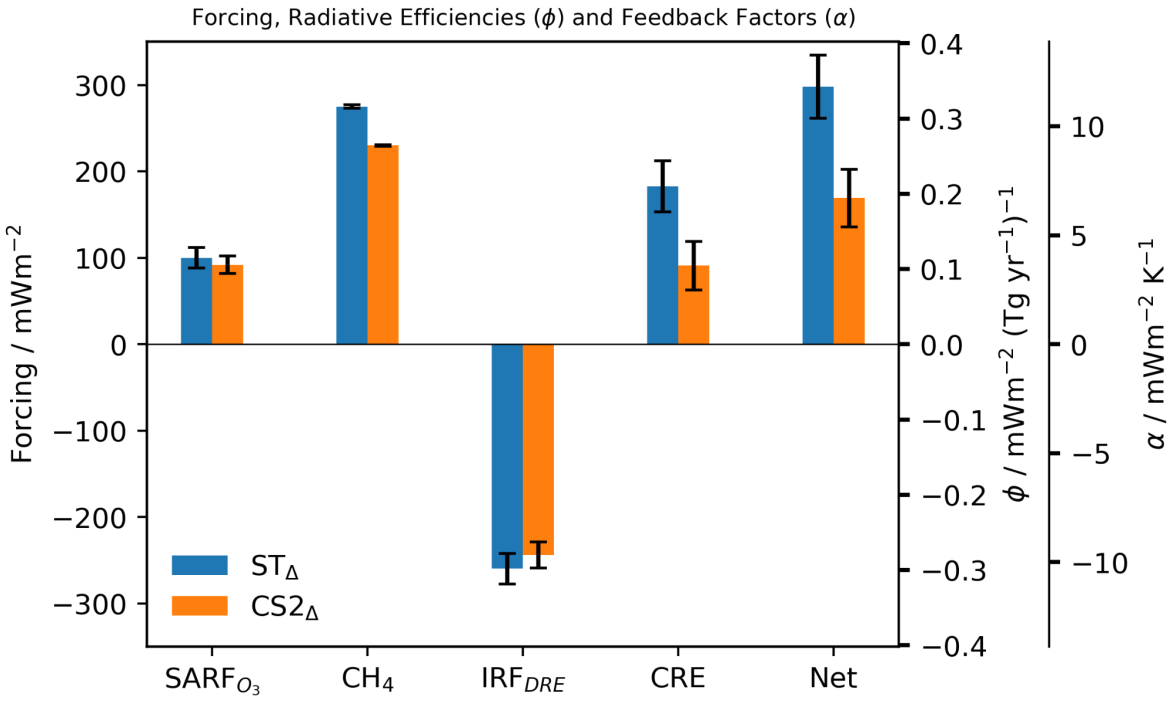

Fig. 1. Forcing, radiative efficiency (ϕ) and feedback factor (α) for individual components and their combined totals (Net) for ST$_\Delta$ and CS2$_\Delta$.

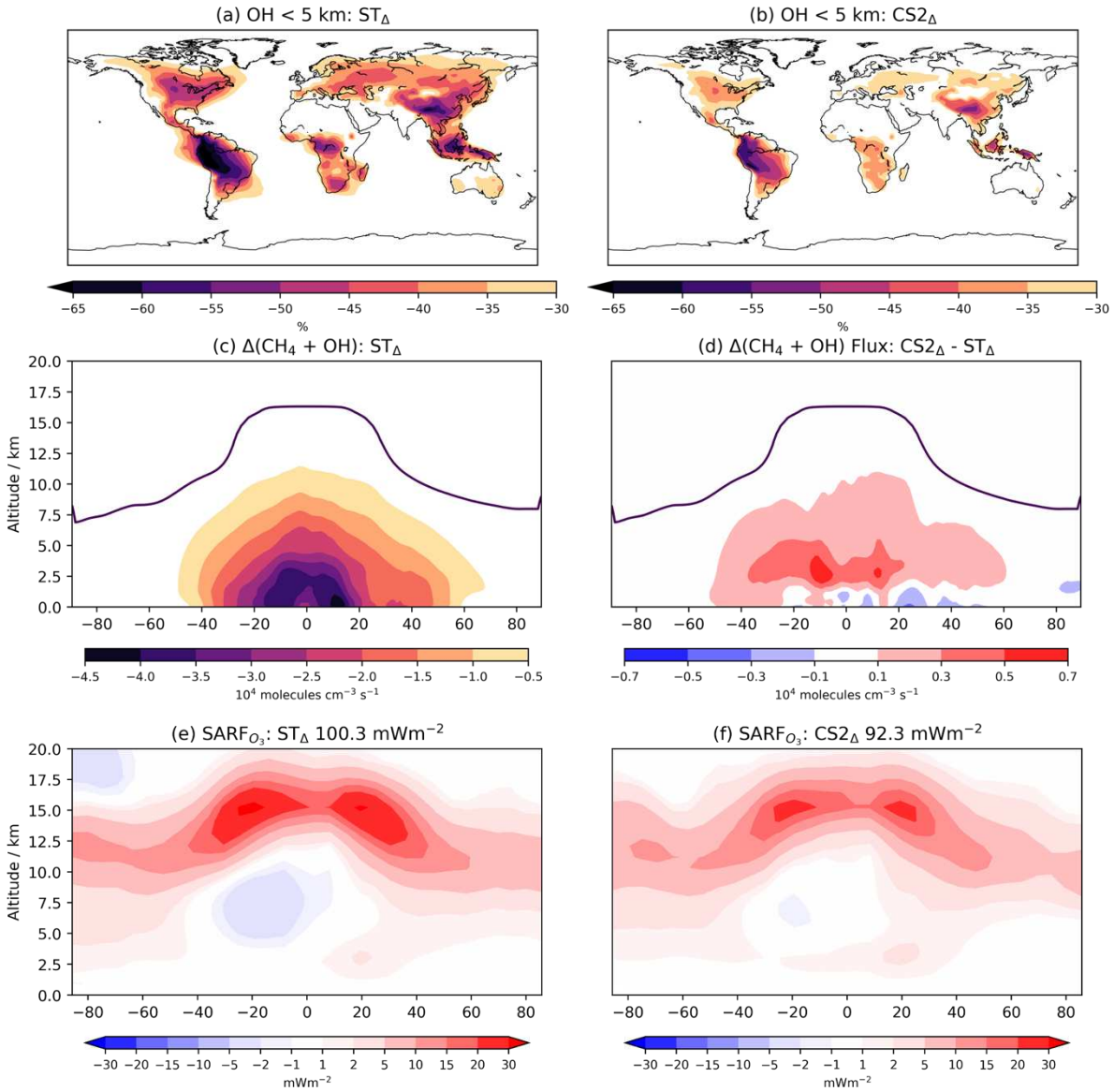

Fig. 2. Percentage change in OH in lowest 5 km for (a) ST_Δ and (b) $CS2_\Delta$. Change in CH_4 oxidation flux for (c) ST_Δ and (d) $CS2_\Delta$ - ST_Δ. Forcing from O_3 changes for (e) ST_Δ and (f) $CS2_\Delta$, values in title show global mean forcing.

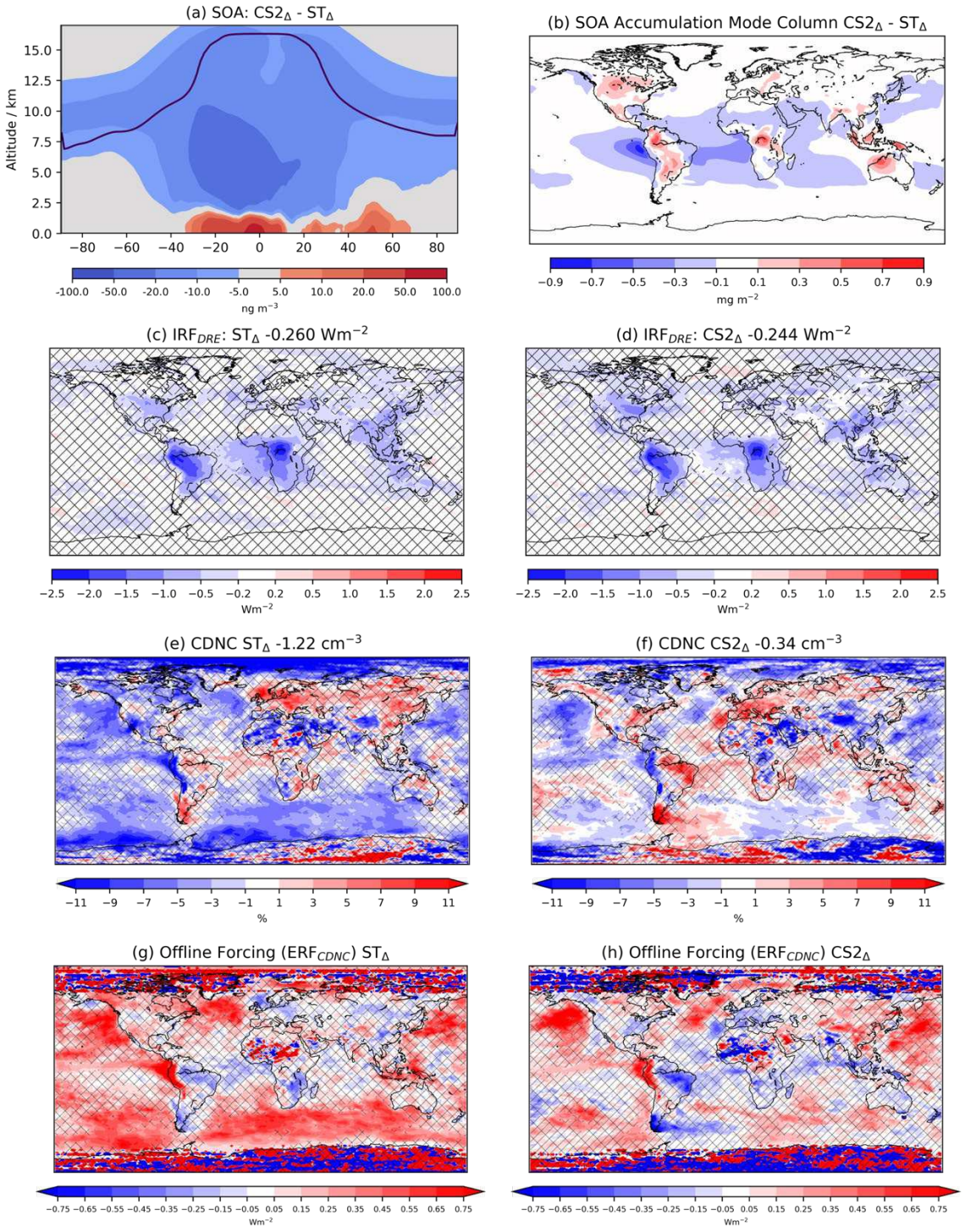

Fig. 3. Difference in (a) zonal mean SOA increase and (b) accumulation mode SOA column increase between $CS2_{\Delta}$ and ST_{Δ}. IRF_{DRE} for (c) ST_{Δ} and (d) $CS2_{\Delta}$. Percentage change in vertically averaged CDNC concentration (e) ST_{Δ} and (f) $CS2_{\Delta}$ and forcing due to change in CDNC (ERF_{CDNC}) for (g) ST_{Δ} and (h) $CS2_{\Delta}$ calculated using the offline approach of Grosvenor and Carslaw (2020) (Methods). Values in titles are global mean forcing (c,d) and CDNC change (e,f). Non-hatched regions in (c-h) show areas where the change is statistically significant (95% confidence).

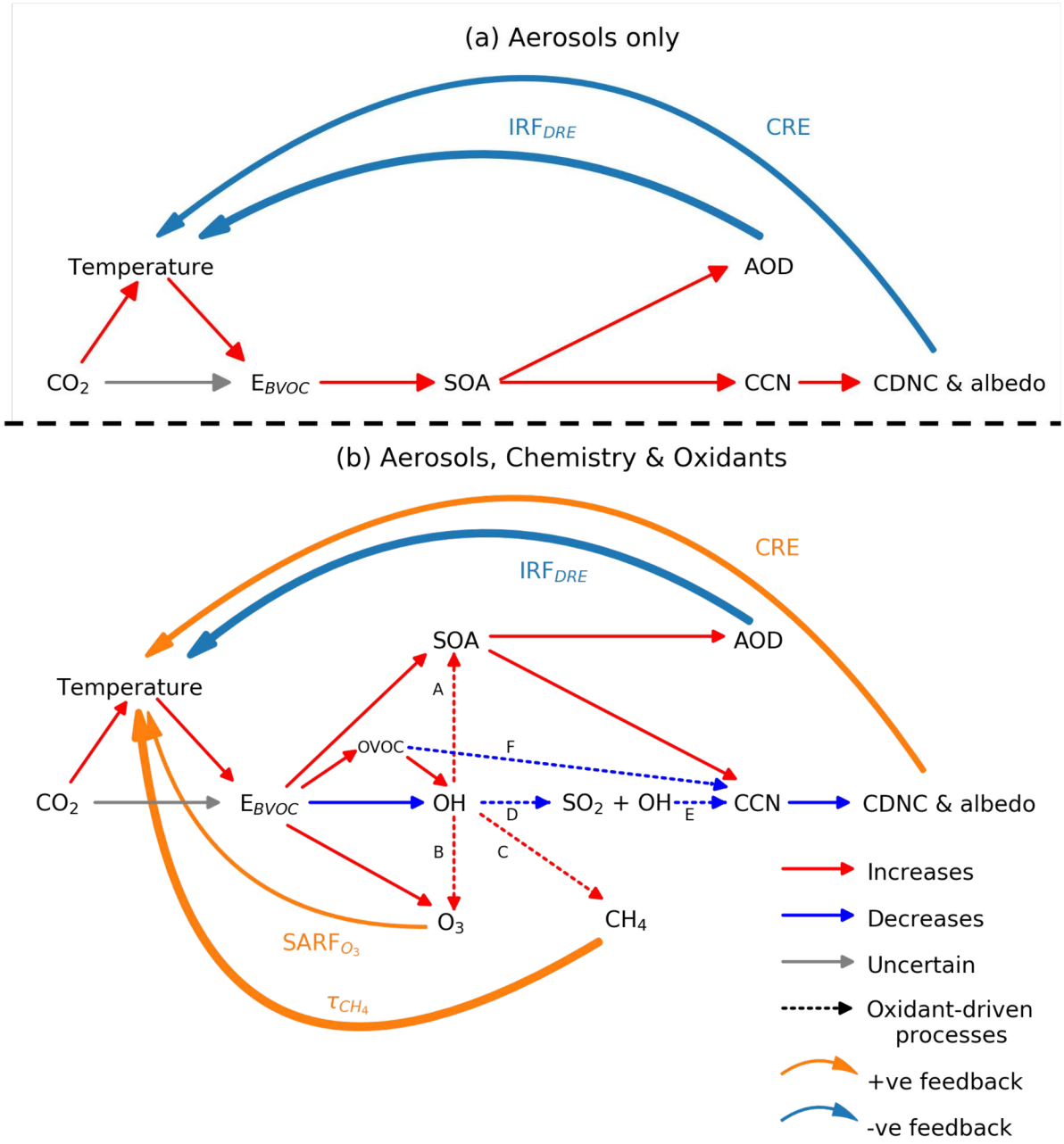

Fig. 4. Atmospheric composition response and BVOC feedback from an increase in CO_2 when (a) only aerosols are considered yielding a negative feedback (adapted from Sporre et al., 2019) and (b) when chemistry and oxidants are also allowed to respond, leading to a more complex response. Aerosol optical depth (AOD) is a measure of aerosol scattering. Dashed lines in (b) show important oxidant-driven responses including reduced OH driving (A) increased SOA lifetime and climatic impact, (B) greater vertical transport of O_3 precursors and thus O_3 forcing, (C) increased CH_4 lifetime and climatic impact, (D, E) reduction in gas phase SO_2 oxidation with attendant decreases in H_2SO_4, new particle formation, CDNC and cloud albedo and (F) additional H_2O_2 from BVOC oxidation products (OVOC) favouring addition of mass to existing aerosol via in-cloud SO_2 oxidation.

Supplementary Files

This is a list of supplementary files associated with this preprint. Click to download.

- InventoryofSupportingInformation.docx